# Demonstration of the GC-Rich Common Arm in Yeast Ribosomal 5.8S RNA via 500-MHz Proton Nuclear Magnetic Resonance and Overhauser Enhancements†

Kai Mon Lee and Alan G. Marshall*,‡

*Department of Biochemistry, The Ohio State University, Columbus, Ohio 43210*

*Received May 20, 1986; Revised Manuscript Received July 9, 1986*

ABSTRACT: In this paper we report the first $^1$H NMR study of the base-paired secondary structure of yeast 5.8S RNA. On the basis of a combination of homonuclear Overhauser enhancements and temperature dependence of the proton 500-MHz NMR spectrum, we are able to identify and assign eight of the nine base pairs in the most thermally stable helical arm: $G_{116}$·$C_{137}$–$C_{117}$·$G_{136}$–$C_{118}$·$G_{135}$–$C_{119}$·$G_{134}$–$C_{120}$·$G_{133}$–$U_{121}$·$G_{132}$–$U_{122}$·$A_{131}$–$G_{123}$·$C_{130}$. This arm contains an unusually temperature-stable (to 71 °C) segment of four consecutive G·C base pairs. This work constitutes the most direct evidence to date for the existence and base-pair sequence of the GC-rich helix, which is common to most currently popular secondary structural models for eukaryotic 5.8S ribosomal RNA.

Yeast 5.8S rRNA belongs to a class of small RNA molecules [including transfer RNA (tRNA)] that function in protein synthesis at the ribosome. The structure and function of the smallest RNA, tRNA, are relatively well understood for two reasons. First, the three-dimensional structure of tRNA has been determined crystallographically (Rich, 1977; Kim, 1976) and confirmed in solution via proton NMR [e.g., Reid (1981)]. Second, tRNA is normally found in the free cytoplasm; thus the tRNA solution structure should give a good starting point for describing tRNA bound to the ribosome during peptide chain elongation. In contrast, 5.8S rRNA is normally bound to the ribosome, and its three-dimensional structure has not been attempted by crystallography or via proton NMR.

Eukaryotic 5.8S rRNA is thought to be hydrogen bonded to higher molecular weight ribosomal RNAs [in yeast, to the 25S rRNA from the large ribosomal subunit (Lo & Nazar, 1981)]. 5.8S rRNA can be released from whole ribosomes or ribosomal subunits by application of either heat or denaturants (urea, formamide) without simultaneous release of ribosomal proteins (Nazar, 1978; Giorgini & Delucca, 1976). Nazar (1978) showed that yeast 5.8S rRNA can be reconstituted efficiently into 60S ribosomal subunits from the same species. The ease with which 5.8S rRNA can be dissociated and reincorporated into ribosomal subunits suggests that 5.8S RNA is probably located on or near the surface of the ribosome (Lo & Nazar, 1982; Liu et al., 1983). The region of interaction between 5.8S and 28S rRNA in mouse ribosomes appears to be between the 3′-terminus of the 5.8S rRNA molecule and a Watson–Crick complementary segment of the 28S rRNA molecule and is probably stabilized by the presence of a GC-rich arm near the 3′-terminus of 5.8S RNA (Walker & Pace, 1983; Walker et al., 1982; Peters et al., 1982; Nazar & Sitz, 1980). Although the role of 5.8S RNA in protein synthesis remains as elusive as that of other rRNAs, it has been suggested that 5.8S rRNA is involved in the binding of aminoacyl-tRNA to the ribosome (Ulbrich, 1982; Erdmann, 1976).

The first determination of the *primary* structure of a 5.8S rRNA was reported by Rubin (1973) for yeast. About 38 5.8S rRNA nucleotide sequences have since been reported (Erdmann & Wolters, 1986). All 5.8S rRNA molecules have 157–160 nucleotides, contain modified nucleotides, and show a high degree of sequence homology.

The presence of 5.8S rRNA *secondary* structural segments can be inferred from limited nuclease digestion (Fujiwara & Ishikawa, 1982; Wildeman & Nazar, 1981; Darlix & Rochaix, 1981; Mackay & Doolittle, 1981; Mackay et al., 1980; Olsen & Sogin, 1982; Khan & Maden, 1976; Nazar et al., 1975), Raman spectroscopy (Luoma & Marshall, 1978), chemical modifications (Liu et al., 1983; Lo & Nazar, 1982; Kelly & Maden, 1980; Kelly et al., 1978), and optical and fluorescence experiments (Van et al., 1977). On the basis of consideration of maximal base pairing using Tinoco rules (Gralla & Crothers, 1973), several models for the secondary structure of 5.8S rRNA in solution have been proposed (Rubin, 1973; Nazar et al., 1975; Luoma & Marshall, 1978; Ford & Mathieson, 1978; Uris et al., 1982). All of these models are largely compatible with the above-listed experimental results. On the basis of the above experiments, it has not yet been possible to establish a universal secondary structure for ribosomal 5.8S RNAs.

Proton NMR and homonuclear Overhauser enhancement (NOE) experiments constitute the method of choice for identification and assignment of base pairs in RNAs in solution. First demonstrated for tRNAs (Johnston & Redfield, 1981; Heerschap et al., 1982, 1983a,b; Hare & Reid, 1982a,b; Roy & Redfield, 1983), the method has since been employed for identification of several base-paired secondary structural segments of ribosomal 5S RNAs from both prokaryotes (Kime & Moore, 1983; Kime et al., 1984; Chang & Marshall, 1986a) and eukaryotes (Li & Marshall, 1986; Chen & Marshall, 1986). In this paper we report the first NMR and NOE studies on 5.8S rRNA, including temperature-dependent melting experiments.

## Materials and Methods

*Isolation and Purification of Yeast 5.8S rRNA.* Brewers' yeast (*Saccharomyces carlsbergensis*) cells were generously provided by the Anheuser-Busch Brewery, Inc., Columbus, OH. 5.8S rRNA was extracted from the cells according to the procedure of Rubin (1975). Specifically, yeast cells were suspended in a buffer containing 20 mM ethylenediamine

† This work was supported by grants (to A.G.M.) from the U.S. Public Health Service (NIH 1 R01 GM-29274, NIH 1 S10 RR-01458) and The Ohio State University.

‡ A.G.M. is also a member of the Department of Chemistry.

0006-2960/86/0425-8245$01.50/0 

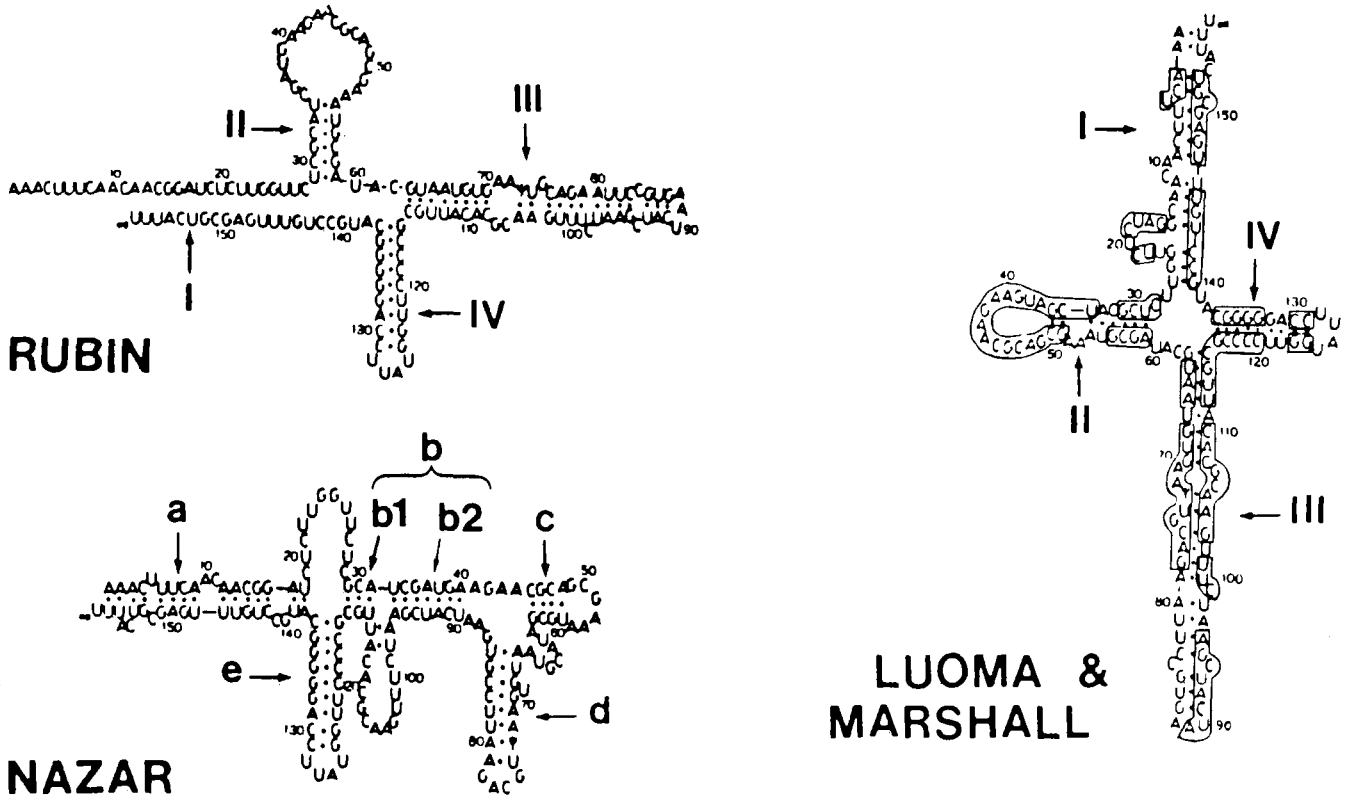


FIGURE 1: Three proposed secondary base-pairing schemes for 5.8S rRNA, each adapted to the primary sequence for *S. cerevisiae*. The circled bases are those that are conserved in all known 5.8S RNA primary nucleotide sequences.

tetraacetic acid (EDTA), 0.1 M sodium acetate, and 1% sodium dodecyl sulfate (SDS) (pH 5.0). One-half volume of phenol was added, and the mixture was stirred vigorously for 2 h at 40–45 °C. The phases were separated by centrifugation at 9800*g*, and the aqueous phase was removed and reextracted with an equal volume of phenol. RNA was then allowed to precipitate overnight at −20 °C after addition of 2.5 volumes of 95% ethanol. The precipitated RNA consisted of tRNAs, 5S rRNA, 5.8S rRNA, and other large rRNAs. Purification via ion-exchange (DEAE-32) and gel filtration (Sephadex G-75) chromatography yielded 5.8S rRNA of purity >92% as determined from 10% acrylamide gel electrophoresis.

*NMR Samples.* Yeast 5.8S rRNA was dissolved in 10 mM EDTA, 100 mM NaCl, and 10 mM sodium cacodylate, pH 7.0, and heated to 65 °C for 10 min to remove metal ions. The solution was allowed to cool slowly to room temperature and then dialyzed against 1 mM EDTA, 100 mM NaCl, and 10 mM sodium cacodylate, pH 7.0, at 5 °C with one change of buffer. The final RNA concentration was adjusted to 56 mg/mL by concentrating the dialyzed RNA sample via ultrafiltration via an Amicon Centricon apparatus. $D_2O$ was added to give a final 5% $D_2O$ concentration, to provide a $^2D$ field-frequency lock signal.

*NMR Spectroscopy.* All spectra were obtained with a Bruker AM-500 Fourier transform nuclear magnetic resonance (FT NMR) spectrometer, with phase-cycled quadrature detection. Chemical shifts were measured relative to $H_2O$ and referred to DSS [3-(trimethylsilyl)-1-propanesulfonic acid] from an independent calibration. Downfield shifts are defined as positive.

Water suppression in NMR spectra was achieved via a 1331 hard pulse sequence (Hore, 1983) with the radio frequency carrier centered at the water resonance. The NOE spectra were produced via a modified Redfield 214-pulse sequence (Redfield et al., 1975; Chang & Marshall, 1986a) with the radio frequency carrier located at 15 ppm (i.e., 5100 Hz away from the water resonance). An acquisition period of 100 ms (4K time-domain data) and a relaxation delay of 0.5 s were typical. With either excitation, the final spectrum gave a base line that required only slight flattening.

NOE difference spectra were obtained at relatively low decoupler power (0.50–0.05 mW, corresponding to a bandwidth of 21.4–7.6 Hz), for the purpose of selective saturation (preirradiation period 0.5 s, to prevent extensive spin diffusion) of the resonance of interest, with off-resonance irradiation at 18 ppm. NOE difference spectra were apodized to give a line broadening of 10 Hz in order to enhance the signal-to-noise ratio. In some cases NOE difference spectra were subjected to exponentially time-weighted resolution enhancement to resolve components of a multipeak envelope. NOE experiments were carried out at 22 °C unless otherwise stated, in order to prevent too rapid chemical exchange of hydrogen-bond imino protons with water protons.

## Results and Discussion

Figure 1 shows three proposed secondary base-pairing schemes for 5.8S rRNA, each adapted to the primary nucleotide sequence of *Saccharomyces cerevisiae*. The Rubin and cloverleaf models share a common "helix III", the Nazar and cloverleaf models share most of a common stalk that pairs the 3′- and 5′-termini together, and all three models share a common arm variously labeled as "IV" or "e".

*Absence of 5.8S rRNA Multimers in NMR Samples.* Figure 2 (top) shows the proton NMR spectrum of yeast 5.8S rRNA (ca. 1 mM = 56 mg/mL), in 10 mM cacodylate, 100 mM sodium chloride, and 1 mM EDTA, pH 7.0, in the absence of $Mg^{2+}$. The broad "humps" labeled as A (13.5–14.5 ppm) and K (10.8–11.2 ppm) correspond to the respective regions in which AU and GU base-pair hydrogen-bond imino protons are normally found. In order to ascertain whether or not these broad envelopes were due to homogeneous broadening arising from long rotational correlation times associated

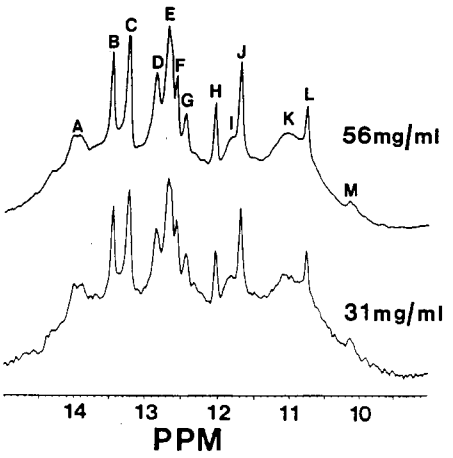


FIGURE 2: 500-MHz proton NMR spectra of yeast 5.8S rRNA at two RNA concentrations: (top) 56 mg/mL; (bottom) 31 mg/mL. All NMR samples contained 95%/5% $H_2O/D_2O$, 100 mM NaCl, 1 mM NaEDTA, and 10 mM sodium cacodylate, pH 7.0.

with RNA aggregates resulting from too high RNA concentration, we diluted the RNA sample to a concentration of 31 mg/mL. The close similarity between the proton NMR spectra of the dilute sample (Figure 2, bottom) and the concentrated sample (Figure 2, top) shows that the broad spectral features at A and K are due to either superposition of several unresolved resonances or rapid exchange of base-pair protons with $H_2O$ rather than to RNA aggregation. In support of this view, independent gel electrophoresis of our 31 and 56 mg/mL samples showed no bands with mobility slower than that of 5.8S RNA, even for high sample loads. Rapid exchange might be expected from rapid opening and closing of the least stable helix (e.g., helix I with 7 A·U and 3 G·U base pairs in the cloverleaf or Nazar models of Figure 1), particularly since $Mg^{2+}$ had been removed from our RNA NMR samples.

*Multistage Unfolding of 5.8S RNA.* Differential scanning calorimetry (DSC) has revealed multistage heat-induced unfolding of tRNAs (Privalov & Filimonov, 1978) and 5S RNAs (Li & Marshall, 1985; Chang & Marshall, 1986b). Analysis of the DSC curves into a sum of two-state melting stages yields component enthalpies of melting, some of which can be interpreted in terms of thermodynamic stabilities calculated from Tinoco rules (Gralla & Crothers, 1973) for particular base-paired helices in those molecules. The differential thermal melting curve for yeast 5.8S RNA in the absence of $Mg^{2+}$ has been analyzed into three to five transitions (Maruyama et al., 1983); however, the component enthalpies of melting for each stage correlate poorly with those calculated for individual helices of any of the base-pairing schemes shown in Figure 1. In both the DSC and differential thermal melting experiments, one monitors a single parameter (heat capacity or optical absorbance) that is a sum of effects from the whole molecule. From 500-MHz proton NMR at several temperatures, on the other hand, we can monitor RNA unfolding simultaneously at each of the many (ca. 15–20) resolved peak positions in the spectrum.

Figure 3 shows the stepwise melting of yeast 5.8S rRNA, as reflected in the stability of its base-pair hydrogen bonds detected via 500-MHz proton NMR spectrometry. The close similarity between NMR spectra taken before and after exposure of yeast 5.8S rRNA to high temperature (91 °C for 30 min or 61 °C for 48 h) is clearly evident in Figure 4. Since the NMR spectrum is highly sensitive to any changes in base pairing, the results of Figure 4 show that a near-identical base-pair structure is regained after heating and cooling the 5.8S rRNA. Because the observed structural changes are

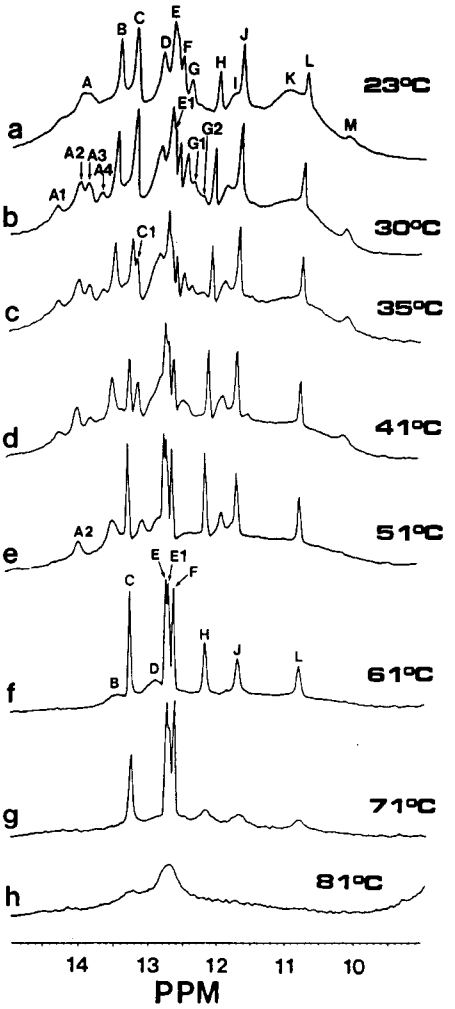


FIGURE 3: 500-MHz proton NMR spectra of yeast 5.8S rRNA at several temperatures.

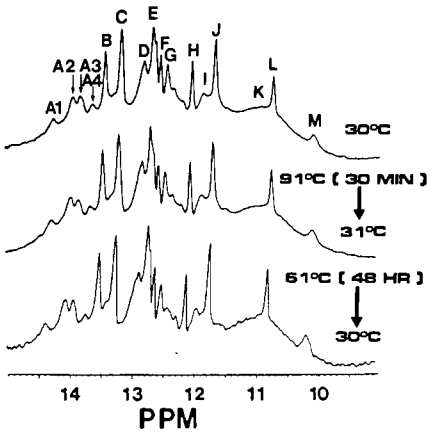


FIGURE 4: Reversibility of yeast 5.8S rRNA heat-induced unfolding: (top) initial spectrum at 30 °C; (middle) spectrum for sample that had been heated to 91 °C for ca. 30 min and then allowed to cool to 31 °C; (bottom) spectrum for sample that had been maintained at 61 °C for 48 h and then allowed to cool to 30 °C.

reversible, we can confidently analyze the thermal melting of yeast 5.8S rRNA in terms of chain unfolding rather than chain breaking. Similar results have been seen for 5S RNAs in the absence of $Mg^{2+}$ (Li & Marshall, 1985; Chang & Marshall, 1986b).

Although 5.8S rRNA from rat or chicken liver is known to dimerize at ≥67.5 °C at RNA concentrations as low as 0.8 mg/mL from gel electrophoresis (Sitz et al., 1978) and hydrodynamic (Behlke et al., 1985) experiments, yeast 5.8S

Table I: Free Energies of Stability for Individual Helices Computed from Tinoco Rules (Gralla & Crothers, 1973) for Three Proposed Secondary Structures of Yeast 5.8S Ribosomal RNA

| helix | $\Delta G$ (kcal/mol) |
|---|---|
| | Cloverleaf Model (Luoma & Marshall, 1978) |
| I | −2.0 (including bulges and interior loop) |
| II | −8.4 (including hairpin and bulge) |
| III | −5.1 (including hairpin, bulges, and interior loops) |
| IV (GC-rich arm) | −20.6 (including hairpin loop) |
| | Burp Gun Model (Nazar et al., 1975) |
| a | −3.1 (including bulges and interior loop) |
| b | −15.4 (including 16-base bulge) |
| c | −3.4 (including hairpin loop) |
| d | −1.1 (including hairpin loop and bulge) |
| e (GC-rich arm) | −20.6 (including hairpin loop) |
| | Rubin Model (Rubin, 1973) |
| I | (bases not paired) |
| II | −5.3 (including hairpin loop) |
| III | −5.1 (including hairpin, bulges, and, interior loops) |
| IV (GC-rich arm) | −20.6 (including hairpin loop) |

rRNA was found to dimerize only to a small extent (ca. 5%) independent of incubation temperature. Consistent with those results, we find no NMR evidence for the formation of multimers of yeast 5.8S rRNA at elevated temperature at the RNA concentrations used for NMR experiments.

*Calculated Thermal Stabilities of 5.8S rRNA Base-Paired Helical Segments.* In order to identify particular proton NMR resonances from the temperature dependence of their line widths and intensities, we must first estimate the relative thermal stabilities of various base-paired arms of the 5.8S rRNA secondary structure. Free energies calculated from Tinoco rules (Gralla & Crothers, 1973) are listed in Table I for each of the helical arms of the three secondary structures shown in Figure 1. The entries in Table I should not be taken too literally, because (a) the stability for tertiary structural elements (currently unknown) cannot be estimated, (b) fraying at the ends of the short helical segments may affect the helical stability, and (c) cooperative folding can result in well-resolved melting transitions that do not correspond to independent melting of individual isolated helical segments.

Nevertheless, an important prediction from Table I is that the most stable helix (ca. 20 kcal/mol stability free energy) is the GC-rich arm that is common to all three of the secondary base-pairing schemes. By comparison, the "stem" helix (labeled as "I" or "a" in the models) is predicted to be weakly paired (<5 kcal/mol stability free energy), in accord with limited pancreatic and T1 ribonuclease digestion (Wildeman & Nazar, 1981) and evidence for intermolecular contacts involving the 3′- and 5′-termini of 5.8S RNA in the 5.8S/28S complex from mouse (Walker & Pace, 1983; Pace et al., 1977; Walker et al., 1982, 1983).

*Identification of GC-Rich Arm Base Pairs from High-Temperature Proton NMR.* Figure 3 shows 500-MHz proton FT NMR spectra of yeast 5.8S rRNA as a function of temperature. As the temperature increases, each of the base-pair hydrogen-bonded imino proton resonances begins to lose intensity and broaden due to increased rate of chemical exchange with water. Loss of intensity or "melting" in the NMR spectrum occurs when the lifetime of a particular base pair with respect to opening drops to 1–5 ms (Reid, 1979; Kearns, 1976; Crothers et al., 1974). The "melting out" of a particular base-pair proton resonance therefore reflects both an equilibrium effect (i.e., fraction of the time that a base-pair proton spends in its base pair rather than on an $H_2O$ molecule) and a kinetic effect (increased line broadening with increased off-rate constant for chemical exchange). DSC and optical melting curves, on the other hand, measure the equilibrium fraction of bases that are unpaired or unstacked, respectively.

Since the GC-rich arm is predicted to be highest in thermodynamic stability (Table I), it is reasonable to expect that it should unfold at a higher temperature than other secondary structural segments. Moreover, NMR peaks arising from adjacent secondary base pairs in the same helical segment are expected to melt at similar temperatures. Our strategy is therefore to pick out proton resonances that persist at the highest temperatures as belonging to GC-rich arm base pairs and then use proton homonuclear Overhauser enhancement experiments (at lower temperature) to identify (e.g., A·U, G·C, or G·U) those peaks and assign them to particular primary nucleotide sequence positions.

In contrast to 5S rRNAs, whose base-pair hydrogen-bond imino proton resonances typically melt out completely at ca. ≥60 °C, yeast 5.8S rRNA exhibits at least seven well-resolved imino proton resonances that persist at 61 °C (peaks C, E, E1, F, H, J, and L in Figure 3f). Peaks B and D are partly melted but still visible at 61 °C.

The GC-rich arm with a net stability of −21 kcal/mol should be the last secondary feature to melt at high temperature. Integration of the 61 °C spectrum (Figure 3f) yields approximately 8 base-pair protons, in reasonable agreement with the 10 base-pair protons (the G·U pair contributes 2 NMR-observable base-pair protons) expected for the GC-rich arm. The absence of 1–2 NMR-observable base-pair protons could be due to end fraying (Boyle et al., 1980; Heus et al., 1983) of terminal GC base pairs $G_{116}$·$C_{137}$ and/or $G_{124}$·$C_{129}$.

*Assignment of GC-Rich Arm Base Pairs from Temperature Dependence of Proton NMR Spectra.* On the basis of their exceptional thermal stability, the four well-resolved resonances remaining at 71 °C (peaks, C, E, E1, and F in Figure 3g) almost certainly correspond to the four consecutive G·C base pairs, $C_{117}$·$G_{136}$ to $C_{120}$·$G_{133}$, of the GC-rich arm. On the basis of its relatively large downfield chemical shift (13.45 ppm) and somewhat lower melting temperature, peak B can tentatively be assigned to $U_{122}$·$A_{131}$. Similarly, peak D might be a terminal $G_{116}$·$C_{137}$ or $G_{124}$·$C_{129}$, since terminal base pairs are much more susceptible to opening than internal base pairs.

The simultaneous broadening at 71 °C of the three resonances J, L, and H (Figure 3g) suggests that they may lie close together in the next most stable segment of the GC-rich arm (see Figure 1). Peaks J/L can be assigned to $U_{121}$·$G_{132}$ on the basis of their common melting temperature and their chemical shifts, which fall in the 10.0–12.5 ppm range that is typical for G·U imino protons (Johnston & Redfield, 1978; Chang & Marshall, 1986a). Peak H would then most likely be $G_{123}$·$C_{130}$ because of its common melting with the adjacent $U_{122}$·$A_{131}$ base pair (peak B) and next nearest $U_{121}$·$G_{132}$ base pair (peaks J/L).

The difference spectrum between 61 and 71 °C (Figure 5, middle) clearly shows that peaks C and E1 begin to melt before peaks E and F. We might therefore anticipate that peaks C and E1 represent the two endmost remaining base pairs ($C_{117}$·$G_{136}$ and $C_{120}$·$G_{133}$) of the four consecutive G·C's in the GC-rich arm. The above assignments can next be confirmed via proton NOE experiments (see below). Finally, scrutiny of the spectra from lower temperatures (Figure 3a–e) reveals a multistage (rather than totally cooperative) melting process. However, in the absence of more complete identification and assignment of the base-pair protons involved, we are not yet in a position to analyze those changes in terms of the unfolding

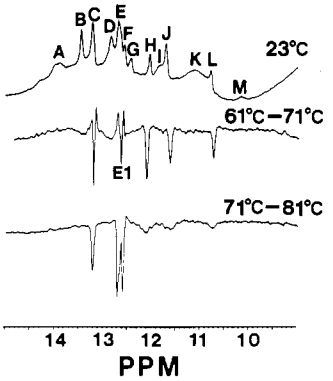


FIGURE 5: 500-MHz proton NMR difference spectra between yeast 5.8S rRNA spectra acquired at different temperatures: (top) room temperature spectrum; (middle) difference spectrum between 61 and 71 °C; (bottom) difference spectrum between 71 and 81 °C. A negative peak in the difference spectrum corresponds to a resonance that melts away in proceeding from the lower to the higher temperature.

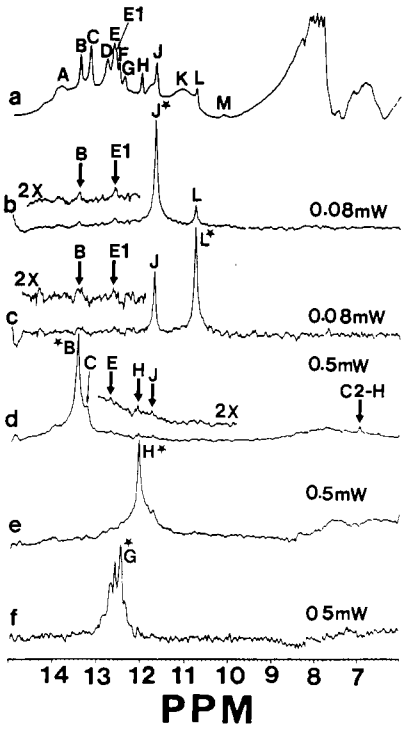


FIGURE 6: Proton 500-MHz FT NMR spectrum (a) and proton homonuclear Overhauser difference spectra (b–f) resulting from irradiation of peaks J, L, B, H, and G at 22 °C. In each case, the irradiated peak is denoted by a star (★) and decoupler power is shown at the right.

of particular secondary helical segments.

*Base-Pair Sequencing of the GC-Rich Arm via Proton NOE Connectivity.* As discussed extensively in previous papers on 5S rRNA from this laboratory (Li & Marshall, 1986; Chang & Marshall, 1986a; Chen & Marshall, 1986), NOE difference spectra provide for identification (A·U, G·C, or G·U) and next nearest base-pair assignment for RNA base pairs. In particular, a G·U pair affords a good starting point (Chang & Marshall, 1986a) because of its relatively upfield chemical shift and the strong NOE's between its two NMR-observable imino hydrogen-bond base-pair protons. The strong mutual NOE's observed via irradiation of peaks J and L (Figure 6b,c) clearly confirm their prior identification as $U_{121}$·$G_{132}$ from temperature dependence (Figure 3f). As usual for G·U pairs in tRNAs (Hurd & Reid, 1979; Johnston & Redfield, 1981; Hare & Reid, 1982a,b) and 5S rRNAs (Li & Marshall, 1986; Chang

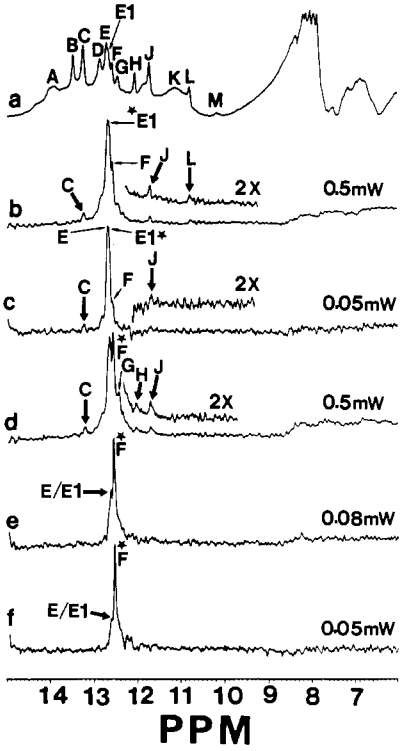


FIGURE 7: 500-MHz proton homonuclear Overhauser difference spectra of yeast 5.8S rRNA, produced as in Figure 6, for peaks E1 and F.

& Marshall, 1986a; Chen & Marshall, 1986), the enhancement from irradiation of the G imino proton (peak L in this case) is larger than that from irradiation of the U imino proton (peak J).

Figure 6b,c also shows weak NOE connectivity from peaks J/L to peaks E1 (12.66 ppm) and B (13.47 ppm). Peak B is clearly an A·U base pair, on the basis of its narrow adenine–C2 proton NOE difference peak at 6.94 ppm (Figure 6d). Moreover, the A·U at peak B gives the expected weak NOE coupling back to peak J (11.73 ppm). Since there is only one A·U pair in the GC-rich arm and since NOE shows that the A·U is next to $U_{121}$·$G_{132}$, peak B must be $U_{122}$·$A_{131}$.

Peaks E/E1 include several overlapping hydrogen-bond proton resonances. Nevertheless, Figure 7b,c shows that irradiation at peaks E and E1 (35 Hz apart, with E1 at 12.66 ppm) gives clear NOE's to peaks J/L (11.71/10.77 ppm) and C (13.24 ppm). The reverse experiments (Figures 6b,c and 8d) reveal that peaks J/L are NOE coupled to peak E1, whereas peak C is NOE coupled to peak E. Since peak E1 shows primary NOE behavior characteristic of a G·C imino proton, we can now extend our base-pair sequence to $C_{120}$·$G_{133}$ (E1)–$U_{121}$·$G_{132}$ (J/L)–$U_{122}$·$A_{131}$ (B). It is interesting that irradiation of this G·U elicits NOE's to base pairs on *both* sides of the G·U, since NOE's have previously been observed only to the 3′-side of G in a G·U pair (Heus et al., 1983; Chang & Marshall, 1986a).

Next, since peaks C and E are both G·C's (Figures 7b,c and 8d,e) and since both are stable to 71 °C (Figure 3g), they must correspond to two consecutive base pairs from the GC-rich arm. Furthermore, since peaks C and E are adjacent G·C's, since peaks C, E, E1, and F are the most temperature-stable base-pair protons in the GC-rich arm, and since peak E1 is $C_{120}$·$G_{133}$, it is reasonable to infer that peaks C, E, E1, and F correspond to the tightly stacked segment of four consecutive G·C pairs: $C_{117}$·$G_{136}$–$C_{118}$·$G_{135}$–$C_{119}$·$G_{134}$–$C_{120}$·$G_{133}$. In agreement with that assignment, Figure 9b,c shows that the NOE connectivity between peaks C and E is conserved at

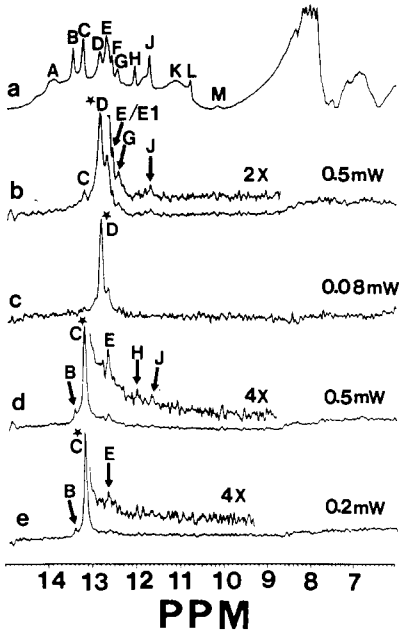


FIGURE 8: 500-MHz proton homonuclear Overhauser difference spectra of yeast 5.8S rRNA, produced as in Figure 6, for peaks D and C.

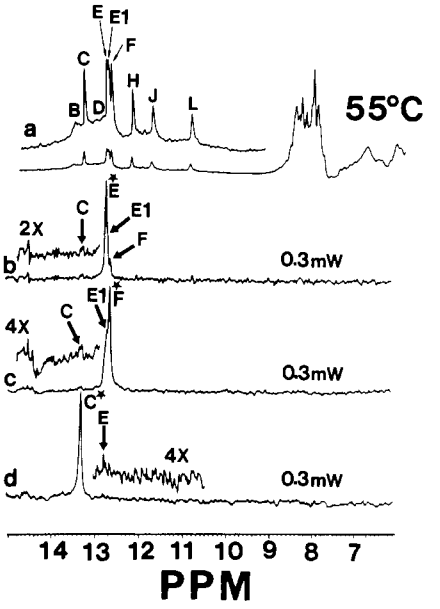


FIGURE 9: 500-MHz proton homonuclear Overhauser difference spectra of yeast 5.8S rRNA, produced as in Figure 6 but at 55 °C, for peaks E, F, and C.

Table II: Assignments for Imino Proton Resonances from the GC-Rich Arm of Yeast 5.8S rRNA and Approximate (±5 °C) Temperature for Onset of Melting for That Base Pair

| resonance | chemical shift (ppm) | base pair | melting temp (°C) |
|---|---|---|---|
| D | −12.85 | $G_{116}$·$C_{137}$ | 41 |
| C | −13.24 | $C_{117}$·$G_{136}$ | 71 |
| E | −12.70 | $C_{118}$·$G_{135}$ | 81 |
| F | −12.57 | $C_{119}$·$G_{134}$ | 81 |
| E1 | −12.66 | $C_{120}$·$G_{133}$ | 71 |
| J/L | −11.70/−10.77 | $U_{121}$·$G_{132}$ | 51 |
| B | −13.47 | $U_{122}$·$A_{131}$ | 51 |
| H | −12.05 | $G_{123}$·$C_{130}$ | 61 |

higher temperature (55 °C), even at low irradiation power (Figure 9d).

It is next necessary to decide the order among G·C pairs corresponding to peaks C, E, E1, and F. The possibilities are C-E-F-E1, E-C-F-E1, F-C-E-E1, and F-E-C-E1. Since irradiation at peak C gives an NOE difference peak at E but not at peaks E1 or F, all but the first arrangement are ruled out, leaving $C_{117}$·$G_{136}$ (C)–$C_{118}$·$G_{135}$ (E)–$C_{119}$·$G_{134}$ (F)–$C_{120}$·$G_{133}$ (E1)–$U_{121}$·$G_{132}$ (J/L)–$U_{122}$·$A_{131}$ (B) as the only possible NOE-consistent assignment. Another argument in favor of peak C as $C_{117}$·$G_{136}$ is its relatively downfield chemical shift (see Table II); a G·C pair stacked in between G·C's on either side would be expected to lie more upfield than 13.24 ppm (Arter & Schmidt, 1976). It is not possible to confirm the E-F-E1 connections directly via one-dimensional NOE, because of too close overlap between those resonances (see Figures 7b–f and 9b,c).

There are two to three possible locations for peak H, the most stable (Figure 3f) remaining unassigned resonance attributed to the GC-rich arm: $G_{116}$·$C_{137}$ (adjacent to peak C), $G_{123}$·$C_{130}$ (adjacent to peak B), and $G_{124}$·$C_{129}$ [terminating into the hairpin loop (see Figure 1)]. Direct irradiation at peak H (Figure 6e) is not especially informative, since H represents a superposition of at least two resonances. However, irradiation at peak B (Figure 6d) gives a difference peak at H and J. Although irradiation at peak C also gives a small difference peak at H (Figure 8d), the same spectrum shows a small difference peak at J, which is four base pairs distant from the base pair previously assigned to C. Therefore, it would appear that irradiation centered at peak C spills over partly to peak B, which is already known to be NOE coupled to peak J (and L); moreover, at 55 °C (a temperature at which peak B has virtually melted out) irradiation at peak C gives only an NOE difference peak at E, with no difference peak at H and J (Figure 9d). On the basis of these results, we assign peak H as $G_{123}$·$C_{130}$ (adjacent to peak B), consistent with the common melting temperature of peaks H and J/L (which is one base pair removed from peak H in the GC-rich arm).

From here on, further assignments must be viewed as somewhat speculative. Irradiation of the remaining resonance, which is stable at high temperature (peak D in Figure 3e,f), gives a difference peak at C, which is likely due in part to power spillover (since the difference peak at C is much reduced when irradiation power is decreased in Figure 8c) but which suggests that peak D could be $G_{116}$·$C_{137}$. The remaining GC-rich arm base pair, $G_{124}$·$C_{129}$, evidently has lower thermal stability and is not NMR visible at elevated temperatures.

In summary, we have combined 500-MHz proton NMR temperature dependence and homonuclear Overhauser enhancements to identify and assign eight of the nine base pairs in the GC-rich arm of yeast 5.8S rRNA: $G_{116}$·$C_{137}$ (D)–$C_{117}$·$G_{136}$ (C)–$C_{118}$·$G_{135}$ (E)–$C_{119}$·$G_{134}$ (F)–$C_{120}$·$G_{133}$ (E1)–$U_{121}$·$G_{132}$ (J/L)–$U_{122}$·$A_{131}$ (B)–$G_{123}$·$C_{130}$ (H). This work constitutes the most direct evidence to date for the existence of a GC-rich arm that is common to most currently popular secondary structural models for 5.8S rRNA. Table II lists the assignments for each base pair, along with the melting onset temperature for each peak. As expected, resonance D, assigned as terminal $G_{116}$·$C_{137}$, exhibits the lowest melting temperature. The next most stable base pairs are peaks B and J/L, assigned as the adjacent A·U and G·U pairs in the GC-rich arm, consistent with the lower expected stability of A·U and G·U compared to G·C base pairs. The opening of the G·U and A·U pairs would be expected to weaken the adjacent $G_{123}$·$C_{130}$, which displays the next highest melting temperature. The four consecutive G·C pairs are all extremely temperature stable, but the two interior pairs melt at a slightly higher temperature than the two exterior pairs of that segment. The

overall conclusion is that the GC-rich arm melts from either end and interior A·U and G·U pairs melt before interior G·C pairs.

Although we are confident that we have identified most of the base pairs in the GC-rich arm of yeast 5.8S RNA, an unequivocal assignment of an extended base-pair sequence in an RNA of molecular weight >50 000 is not possible without additional experiments. Future experiments on 5.8S rRNAs might be directed at comparing different biological species with (slightly) different primary nucleotide sequences and/or isolation of enzyme-cleaved fragments (Lightfoot, 1978) as aids in identifying this and other base-paired helical segments of the molecule.

ACKNOWLEDGMENTS

We thank Dr. C. E. Cottrell for advice on NMR experiments and Anheuser-Busch Brewery, Inc., of Columbus, OH, for providing yeast cells.

REFERENCES

Arter, D. B., & Schmidt, P. G. (1976) *Nucleic Acids Res. 3*, 1437–1447.

Behlke, J., Misselwitz, R., & Welfe, H. (1985) *Int. J. Biol. Macromol. 7*, 283–288.

Boyle, J., Robillard, G. T., & Kim, S.-H. (1980) *J. Mol. Biol. 139*, 601–625.

Chang, L.-H., & Marshall, A. G. (1986a) *Biochemistry 25*, 3056–3063.

Chang, L.-H., & Marshall, A. G. (1986b) *Biopolymers 25*, 1299–1313.

Chen, S.-M., & Marshall, A. G. (1986) *Biochemistry 25*, 5117–5125.

Crothers, D. M., Cole, P. E., Hilbers, C. W., & Shulman, R. G. (1974) *J. Mol. Biol. 87*, 63–88.

Darlix, J.-L., & Rochaix, J.-D. (1981) *Nucleic Acids Res. 9*, 1291–1299.

Erdmann, V. A. (1976) *Prog. Nucleic Acid Res. Mol. Biol. 18*, 45–90.

Erdmann, V. A., & Wolters, J. (1986) *Nucleic Acids Res. 14*, r1–r59.

Ford, P. J., & Mathieson, T. (1978) *Eur. J. Biochem. 87*, 199–214.

Fujiwara, H., & Ishikawa, H. (1982) *Nucleic Acids Res. 10*, 5173–5182.

Giorgini, J. F., & DeLucca, F. L. (1976) *Nucleic Acids Res. 3*, 165–175.

Gralla, J., & Crothers, D. M. (1973) *J. Mol. Biol. 73*, 497–511.

Hare, D. R., & Reid, B. R. (1982a) *Biochemistry 21*, 1835–1842.

Hare, D. R., & Reid, B. R. (1982b) *Biochemistry 21*, 5129–5131.

Heerschap, A., Haasnoot, C. A. G., & Hilbers, C. W. (1982) *Nucleic Acids Res. 10*, 6981–7000.

Heerschap, A., Haasnoot, C. A. G., & Hilbers, C. W. (1983a) *Nucleic Acids Res. 11*, 4483–4499.

Heerschap, A., Haasnoot, C. A. G., & Hilbers, C. W. (1983b) *Nucleic Acids Res. 11*, 4501–4520.

Heus, H. A., van Kimmenade, J. M. A., van Knippenberg, P. H., Haasnoot, C. A. G., DeBruin, S. H., & Hilbers, C. W. (1983) *J. Mol. Biol. 170*, 939–956.

Hore, J. (1983) *J. Magn. Reson. 55*, 283–300.

Hurd, R. E., & Reid, B. R. (1979) *Biochemistry 18*, 4017–4024.

Johnston, P. D., & Redfield, A. G. (1978) *Nucleic Acids Res. 5*, 3913–3927.

Johnston, P. D., & Redfield, A. G. (1981) *Biochemistry 20*, 1147–1156.

Kearns, D. R. (1976) *Prog. Nucleic Acid Res. Mol. Biol. 18*, 91–149.

Kelly, J. M., & Maden, B. E. H. (1980) *Nucleic Acids Res. 8*, 4521–4534.

Kelly, J. M., Goddard, J. P., & Maden, B. E. H. (1978) *Biochem. J. 173*, 1–12.

Khan, M. S. N., & Maden, B. E. H. (1976) *FEBS Lett. 72*, 105–110.

Kim, S.-H. (1976) *Prog. Nucleic Acid Res. Mol. Biol. 17*, 182–216.

Kime, M. J., & Moore, P. B. (1983) *Biochemistry 22*, 2615–2622.

Kime, M. J., Gewirth, D. T., & Moore, P. B. (1984) *Biochemistry 23*, 3559–3568.

Li, S.-J., & Marshall, A. G. (1985) *Biochemistry 24*, 4047–4052.

Li, S.-J., & Marshall, A. G. (1986) *Biochemistry 25*, 3673–3682.

Lightfoot, D. (1978) *Nucleic Acids Res. 5*, 3565–3577.

Liu, W., Lo, A. C., & Nazar, R. N. (1983) *J. Mol. Biol. 171*, 217–224.

Lo, A. C., & Nazar, R. N. (1981) *FEBS Lett. 131*, 41–44.

Lo, A. C., & Nazar, R. N. (1982) *J. Biol. Chem. 257*, 3516–3524.

Luoma, G. A., & Marshall, A. G. (1978) *Proc. Natl. Acad. Sci. U.S.A. 75*, 4901–4905.

Mackay, R. M., & Doolittle, W. F. (1981) *Nucleic Acids Res. 9*, 3321–3334.

Mackay, R. M., Spencer, D. F., Doolittle, W. F., & Gray, M. W. (1980) *Eur. J. Biochem. 112*, 561–576.

Maruyama, S., Akazaki, S., Nitta, K., & Sugai, S. (1983) *Int. J. Biol. Macromol. 5*, 26–32.

Nazar, R. N. (1978) *J. Biol. Chem. 253*, 4505–4507.

Nazar, R. N., & Sitz, T. O. (1980) *FEBS Lett. 115*, 71–76.

Nazar, R. N., Sitz, T. O., & Busch, H. (1975) *J. Biol. Chem. 250*, 8591–8597.

Olsen, G. J., & Sogin, M. L. (1982) *Biochemistry 21*, 2335–2343.

Pace, N. R., Walker, T. A., & Schroeder, E. (1977) *Biochemistry 16*, 5321–5328.

Peters, M. A., Walker, T. A., & Pace, N. R. (1982) *Biochemistry 21*, 2329–2335.

Privalov, P. L., & Filimonov, V. V. (1978) *J. Mol. Biol. 122*, 447–464.

Redfield, A. G., Kunz, S. D., & Ralph, E. K. (1975) *J. Magn. Reson. 19*, 114–117.

Reid, B. R. (1979) in *NMR and Biochemistry* (Opella, S. J., & Lu, P., Eds.) pp 91–115, Dekker, New York.

Reid, B. R. (1981) *Annu. Rev. Biochem. 50*, 969–996.

Rich, A. (1977) *Acc. Chem. Res. 10*, 388–395.

Roy, S., & Redfield, A. G. (1983) *Biochemistry 22*, 1386–1390.

Rubin, G. M. (1973) *J. Biol. Chem. 248*, 3860–3875.

Rubin, G. M. (1975) *Methods Cell Biol. 12*, 45–64.

Sitz, T. O., Kao, S.-C., & Nazar, R. N. (1978) *Biochemistry 17*, 5811–5815.

Ulbrich, N., Chan, Y. L., Huber, P. W., & Wool, I. G. (1982) *J. Biol. Chem. 257*, 11353–11357.

Uris, D., Vandenberghe, A., & De Wachter, R. (1982) *Nucleic Acids Res. 10*, 3517–3530.

Van, N. T., Nazar, R. N., & Sitz, T. O. (1977) *Biochemistry 16*, 3754–3759.

Walker, T. A., & Pace, N. R. (1983) *Cell (Cambridge, Mass.)* *33*, 320-322.
Walker, T. A., Johnson, K. D., Olsen, G. J., Peters, M. A., & Pace, N. R. (1982) *Biochemistry 21*, 2320-2329.
Walker, T. A., Endo, Y., Wheat, W. H., Wool, I. G., & Pace, N R. (1983) *J. Biol. Chem. 258*, 333-338.
Wildeman, A. G., & Nazar, R. N. (1981) *J. Biol. Chem. 256*, 5675-5682.

# Parameters Affecting Fusion between Sendai Virus and Liposomes. Role of Viral Proteins, Liposome Composition, and pH

Karin Klappe,[‡] Jan Wilschut,[‡] Shlomo Nir,[§] and Dick Hoekstra*[,‡]

*Laboratory of Physiological Chemistry, University of Groningen, 9712 KZ Groningen, The Netherlands, and Seagram Center for Soil and Water Sciences, Faculty of Agriculture, The Hebrew University of Jerusalem, Rehovot 76100, Israel*

*Received April 17, 1986; Revised Manuscript Received August 1, 1986*

ABSTRACT: A kinetic and quantitative characterization of the fusion process between Sendai virus and phospholipid vesicles is presented. Membrane fusion was monitored in a direct and continuous manner by employing an assay which relies on the relief of fluorescence self-quenching of the probe octadecylrhodamine B chloride which was located in the viral membrane. Viral fusion activity was strongly dependent on the vesicle lipid composition and was most efficient with vesicles solely consisting of acidic phospholipids, particularly cardiolipin (CL). This result implies that the fusion of viruses with liposomes does not display an absolute requirement for specific membrane receptors. Incorporation of phosphatidylcholine (PC), rather than phosphatidylethanolamine (PE), into CL bilayers strongly inhibited fusion, suggesting that repulsive hydration forces interfere with the close approach of viral and target membrane. Virus-liposome fusion products were capable of fusing with liposomes, but not with virus. In contrast to fusion with erythrocyte membranes, fusion between virus and acidic phospholipid vesicles was triggered immediately, did not strictly depend on viral protein conformation, and did not display a pH optimum around pH 7.5. On the other hand, with vesicles consisting of PC, PE, cholesterol, and the ganglioside $GD_{1a}$, the virus resembled more closely the fusogenic properties that were seen with erythrocyte target membranes. Upon decreasing the pH below 5.0, the viral fusion activity increased dramatically. With acidic phospholipid vesicles, maximal activity was observed around pH 4.0, while with $GD_{1a}$-containing zwitterionic vesicles the fusion activity continued to increase with decreasing pH down to values as low as 3.0. This indicates that the fusion susceptibility of the virus at low pH also depends on the molecular properties of the target membrane. Presumably, these properties determine the ability of the viral proteins to interact hydrophobically with the membranes, thus triggering fusion. Fusion between Sendai virus and CL liposomes at low pH was not affected when the virus had been pretreated with trypsin, suggesting that low pH induced fusion was largely mediated by the viral binding protein HN rather than the fusion protein F. It is concluded that, depending on the pH, different mechanisms are operational in the fusion process between Sendai virus and *liposomes*; i.e., fusion with liposomes can, at least partly, be accomplished in a manner which may not bear physiological significance.

Because of their simplicity and the ease of manipulating their composition, liposomes or phospholipid vesicles are widely used as model systems for studying membrane interaction processes as they occur, e.g., during membrane fusion (Papahadjopoulos et al., 1979; Nir et al., 1983; Wilschut & Hoekstra, 1984, 1986). These studies have yielded valuable information on the physicochemical properties of the lipid molecules per se and their role in artificial membrane fusion. Recently, these model membranes have also been introduced as appropriate target membranes for enveloped viruses (Landsberger et al., 1981; Maeda et al., 1981; Haywood & Boyer, 1982, 1984; Hsu et al., 1983; White et al., 1983; Stegmann et al., 1985). Such viruses display membrane fusion activity as an imperative mechanism to deliver their nucleocapsids into host cells for viral replication (Bächi et al., 1977; Choppin & Scheid, 1980; Lenard & Miller, 1983). It has been demonstrated that those enveloped viruses which enter cells by a process of receptor-mediated endocytosis fuse with liposomes at acidic pH (White & Helenius, 1980; White et al., 1983; Maeda et al., 1981; Stegmann et al., 1985). This is consistent with the concept that these viruses fuse in vivo "from within" with the endosomal membrane (Marsh & Helenius, 1984) triggered by the low pH generated in this organelle (Tycko & Maxfield, 1982). Their relatively high fusogenic capacity has greatly facilitated the ability to investigate the fusion between such viruses and liposomes in a kinetic and quantitative manner (Eidelman et al., 1984; Stegmann et al., 1985; Nir et al., 1986a) using a fluorescence assay based upon resonance energy transfer (Struck et al., 1981; Hoekstra, 1982). Efforts to adapt this procedure in order to study the fusion properties of Sendai virus were less successful due to the much less potent fusion capacity of the virus.

Sendai virus, a negative-strand RNA virus, belongs to the family of paramyxoviruses and fuses with biological target

* Correspondence should be addressed to this author.
[‡] University of Groningen.
[§] The Hebrew University of Jerusalem.

0006-2960/86/0425-8252$01.50/0 